Hydrodynamic Characteristics of Dual Rushton Impeller Stirred Vessels

K. Rutherford, K. C. Lee, S. M. S. Mahmoudi and M. Yianneskis
Centre for Heat Transfer and Fluid Flow Measurement, Dept. of Mechanical Engineering, King's College London, Strand, London, WC2R 2LS, England

The flows generated in vessels stirred by two Rushton impellers were investigated in two vessels of diameter (T) 100 and 294 mm with impellers of diameter D = T/3 using flow visualization, power consumption, mixing time, and 360° ensemble-averaged and 1° angle-resolved LDA measurement techniques. The flows depended strongly on the clearance of the lower impeller above the base of the vessel (C1), the separation between the impellers (C2), and the submergence (C3) of the upper impeller below the top of the liquid column height (H). When these distances were varied, three stable and four unstable flow patterns were observed. Comparisons between the two LDA techniques showed that while the 360° ensemble-averaged measurements are useful for characterizing the overall flow structure and turbulence levels in the vessel, care must be exercised when interpreting such data, since in the impeller region they include periodic variations in the mean velocity in addition to the turbulent fluctuations. The trailing vortex structure and flow periodicity produced by the Rushton impellers is shown to decay significantly within a cylindrical region of height 1.2D and radius 1.0D centered around the middle of the vessel, when C1 = C2 = T/3. The turbulence structure within this region is anisotropic, while outside this region it might be considered mostly isotropic. The main flow features scaled well between the vessels.

Introduction

The flowfields in agitated chemical reactors are very complex, having a strongly three-dimensional character with vortical structures that are not always well defined and high turbulence levels in the vicinity of the impellers. When a configuration employing two or more impellers is adopted the flow complexity is greatly increased, especially when a combination of impeller designs are used, each having its own flow characteristics.

A large body of knowledge has been developed on the flow in vessels stirred by a single Rushton impeller. This impeller induces a strong radial discharge stream and is used for a wide range of industrial processes. One of the earliest investigations into the flow generated by such impellers was carried out by Sachs and Rushton (1954), who investigated the flow characteristics of a single impeller configuration using a photographic technique. They reported the presence of a strong radial discharge flow and a variation in the radial velocity component with impeller blade angle (ϕ). Cutter (1966) estimated that approximately 70% of the energy input to the vessel was dissipated in the impeller region and the discharge stream of a Rushton turbine, with the remainder of the energy being dissipated in the bulk flow of the vessel. The formation of a trailing vortex pair behind each blade of a Rushton impeller (shown in Figure 1) was first reported in detail by van't Riet and Smith (1973), who used a camera mounted on a turntable beneath the vessel and rotating synchronously with the impeller, to record the path of tracer particles in the vicinity of the impeller blades. In a subsequent investigation (van't Riet and Smith (1975)) the axis of the trailing vortex was determined for a range of Reynolds numbers ($Re = \rho ND^2/\mu$). van't Riet et al. (1976) reported that measurements obtained in the impeller discharge stream could overestimate the turbulence levels since such measurements can include the variation in the mean velocity due to the passage of the impeller blades, as well as the turbulent fluctuations. They

Correspondence concerning this article should be addressed to M. Yianneskis.

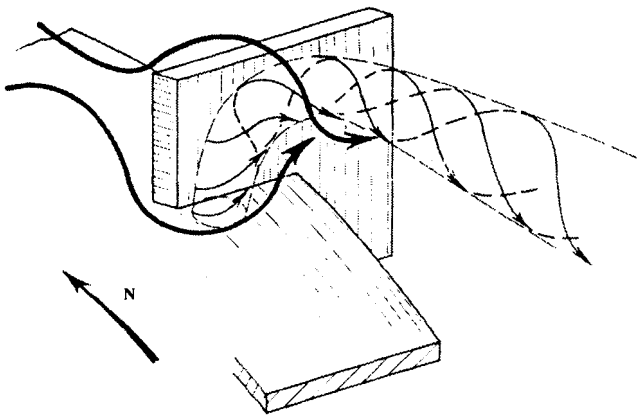

Figure 1. Three-dimensional view of the trailing vortex behind a blade of a Rushton impeller.

fluctuations. They used the term "pseudoturbulence" to describe this nonrandom variation.

More recently, a number of investigators have used laser-Doppler anemometry (LDA) to investigate the flow regime in vessels stirred by a single Rushton turbine since this technique is suitable for the investigation of highly vortical flows, unlike hot-wire anemometry, which cannot resolve the flow direction. Yianneskis et al. (1987) suggested dividing the flow into two regions, namely the impeller region where the flow is periodic and it is necessary to use time- or angle-resolved measurements to describe the flow, and the bulk flow region where ensemble-averaged measurement techniques are appropriate. They also found that the inclination of the impeller stream was dependent on the clearance of the impeller above the base of the vessel, and that 360° ensemble-averaging techniques overpredicted the turbulence in the impeller region by up to 400% due to the influence of the pseudoturbulence. Investigations by Calabrese and Stoots (1989), Wu et al. (1989), Yianneskis and Whitelaw (1993), and Stoots and Calabrese (1994) presented results that quantified the variation of the mean velocities with ϕ due to the passage of each blade of a Rushton impeller and the associated trailing vortex behind the blade.

Although 360° ensemble-averaged measurements include the variation in the mean flow velocity due to the passage of the impeller blades and the associated trailing vortex structure, they are useful since they give a general indication of the mean velocity and turbulence distributions within the stirred vessel. Also, such data provide information suitable for the validation of computational fluid dynamics (CFD) prediction methods, many of which at present do not account for the flow periodicity associated with the passage of the impeller blades as they treat the entire impeller region as a rotating disk.

The flow structure in vessels agitated by dual-impeller configurations is determined predominantly by the flow characteristics of the impeller combinations employed and the degree of interaction that occurs between the impeller streams. Dual-impeller systems are frequently employed in mixing practice and investigations reported to date have been concerned primarily with large impeller clearances and separations, where there is little or no interaction between the flows produced by individual impellers. Such studies have mainly concentrated on the power characteristics (see, for example, Kuboi and Nienow, 1982). The separation distance between the impellers determines the degree of interaction between the impeller discharge streams. When a large separation is employed, around one-half the vessel diameter, the impellers are likely to act independently of each other, with very little interaction occurring between their respective impeller streams. However, when a small separation is used there is a much greater degree of interaction between the discharge flows of the impellers, resulting in complicated, and often unstable, flow patterns. Due to the inherent complexity of such flowfields it has so far proved difficult to predict the characteristics of mixing vessels operating with dual-impeller configurations with certainty. There is no published work known to the authors dealing with the systematic determination of the velocity and turbulence characteristics in configurations where there is strong impeller interaction such as the dual-Rushton study reported here.

One of the aims of the present investigation was to establish the lower impeller clearance and impeller separation values that resulted in stable flow patterns for a dual-Rushton impeller configuration. Three stable and four unstable configurations were identified, and the stable configurations were investigated further using a combination of ensemble-averaged and angle-resolved LDA measurements. For the stable flow configurations the measured Power numbers, mixing times and Flow numbers are presented and discussed. Plots of the ensemble-averaged mean velocity vectors and contours of the kinetic energy of turbulence are presented that show the inclination of the impeller stream for the three configurations, and provide a general indication of the turbulence levels within the vessel. Contours of all three rms velocity components are also shown for one of the stable flow configurations, which was selected for further investigation since it resulted in the lowest mixing-time and power-consumption values of the three stable flow patterns identified. A comparison is conducted between the ensemble-averaged and angle-resolved measurements, and mean velocity vectors and contours of turbulence level are plotted from the angle-resolved LDA data. The position of the axis of the trailing vortex is compared with that in single-impeller configurations determined in previous studies. Comparison of measurements obtained in two vessels of 100-mm and 294-mm diameter is made in order to assess scaling effects in the impeller vicinity.

The results presented provide important information on the characteristics of dual-Rushton impeller configurations as well as LDA data useful for the development of CFD prediction methods. In addition, the anisotropy of the turbulence in the impeller stream region is shown, and the region within which the periodicity associated with the passage of the impeller blades is contained is defined.

Flow Configuration and Experimental Techniques

Flow and vessel configuration

The stirred reactors used in this study were standard configuration cylindrical vessels with four equispaced wall-mounted baffles of width $b = 0.1T$ as shown in Figure 2, where T is the internal vessel diameter, and the liquid column height is $H = T$. Most of the results presented here were obtained in a vessel of diameter $T = 294$ mm with a wall

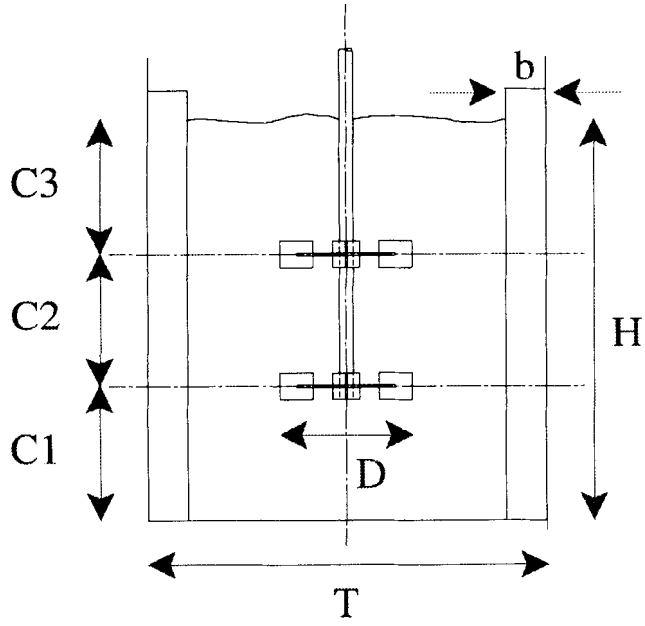

Figure 2. Stirred reactor configuration.

thickness of 3 mm, while measurements were also performed in a vessel of diameter $T = 100$ mm with a wall thickness of 1 mm to investigate the effect of vessel scale, which is an important consideration for the design and performance of a chemical plant.

Full dimensional similarity was achieved between the vessels that were constructed from acrylic plastic (Plexiglas). The design of both vessels incorporated a transparent acrylic base to permit LDA measurements to be performed through either the side wall or the base of the vessel. The cylindrical mixing vessels were located inside square acrylic troughs filled with distilled water in order to minimize the refraction of the laser beams over the outer cylindrical surface of the vessel. Both vessels could be rotated in situ to allow measurements to be performed in different vertical planes.

The impellers used were of diameter (D) equal to one-third of the vessel diameter with the hub of the impeller protruding above and below the impeller disk, and the blades of each impeller were aligned in the same vertical planes, as shown in Figure 2. All features of the impellers, such as the blade height and disk diameter, were also scaled to achieve geometric similarity between the vessels. The impeller blade and disk thickness (t) was 1.0 mm for the 100-mm-diameter tank and 1.65 mm for the 294-mm tank. The effect of impeller thickness ratio (t/D) on the Power number, Flow number, mixing time, mean velocities, and turbulence levels has been investigated in detail by Rutherford et al. (1995) and Mahmoudi (1994) for single and double Rushton impeller configurations and, although finite, it only affects the observation made in this article regarding the scaling of the mean velocities near the impeller tip between the two vessels, as discussed in the corresponding section below.

The experiments were conducted at a Reynolds number (Re) of 40,000, corresponding to an impeller rotational speed of $N = 250$ rpm ($V_{tip} = 1.28$ m/s) in the 294-mm vessel, and $N = 2{,}165$ rpm ($V_{tip} = 3.77$ m/s) in the $T = 100$-mm vessel. Throughout the measurements the impeller speed was monitored using an optical shaft encoder coupled to the impeller shaft, which allowed the impeller speed to be maintained to within ± 0.5 rpm in the 294-mm-dia. vessel, and ± 10 rpm in the 100-mm-dia. vessel, respectively. The impellers rotated in a clockwise direction as viewed from above the vessel. A train of 1,999 pulses and a marker pulse were provided per impeller revolution by the shaft encoder unit, which allowed the instantaneous velocities to be logged according to their respective angular position.

The origin of the coordinate system used is the center of the base of the vessel with $\bar{U}$, $\bar{V}$, $\bar{W}$, and u', v', w' referring to the mean and rms velocities in the axial (z), radial (r), and tangential (θ) coordinate directions, respectively. Polar coordinates r, ϕ are used to represent the location of the LDA measuring volume with respect to the impeller blade pair around which angle-resolved measurements were conducted. For this purpose the center of a reference blade of the lower Rushton impeller was aligned with the marker pulse of the shaft encoder and assigned the impeller blade angle $\phi = 0°$.

A transparent acrylic lid was positioned at a height H equal to the vessel diameter in the $T = 100$-mm vessel, to prevent the entrainment of air bubbles into the flow from the free surface of the liquid, and to permit measurements to be performed in a forward scatter arrangement with the beams entering through the base of the vessel. Two mirrors were positioned on the upper surface of the lid, while the space above the lid was filled with water to ensure that the mirrors were submerged at all times. This arrangement allowed the scattered light to be redirected through 90° by the mirrors and collected using the photomultiplier. The effect of such a lid on the flow in a stirred vessel has been reported previously by Nouri and Whitelaw (1990), who conducted comparisons between flows in vessels with and without lids. They concluded that the use of a lid only affects the flow in the immediate vicinity of the lid/liquid free surface, and the flow velocities were almost identical elsewhere in the vessel.

The laser-Doppler anemometer and experimental methods

Visualization of the flow patterns was carried out using a laser light sheet produced by a 2-W argon-ion laser and a combination of cylindrical and biconvex lenses. Power numbers were measured by determining the torque exerted on the shaft with two strain gauge bridges positioned on the shaft, one between the impellers and one above the upper impeller. The signals from the gauges were acquired and processed with a telemetric system interfaced to a computer (Mahmoudi, 1994).

The LDA was operated in the dual-beam forward-scatter mode, and made use of a 10-mW helium–neon laser. A frequency shift was applied to the two first-order beams through the use of a rotating diffraction grating, and each of the three velocity components was measured separately at each location. The scattered light was collected using a photomultiplier, and the Doppler signals were processed by a TSI model 1990 frequency counter interfaced to a computer.

Two types of LDA measurements were performed in order to characterize the flow structure within the vessels. The first of these was ensemble-averaged measurements performed over the entire revolution of the impellers. During the acquisition of such data, the counter accepted all validated Doppler

signals arriving over 360° of impeller revolution, and the mean and rms velocities were calculated from the ensemble-averaged values. The second was angle-resolved LDA measurements, performed over 60° of impeller revolution by arranging the velocity measurements into 1° angular intervals, from which the mean and rms velocities were calculated. During these measurements the frequency counter would only accept velocity data obtained during a specified 60° interval (between two neighboring impeller blades), over a number of impeller revolutions. It has been established by Lee et al. (1995) that providing a statistically appropriate number of data are obtained per 1° interval, this method provides an accurate picture of the flow structure within the vessel, since the effect of the variation in the mean flow velocity due to the flow periodicity is not included in the rms velocity measurements. The number of data required per 1° interval depends on the local turbulence intensity and was determined to be at least 500 for most measurement locations.

All of the measurements reported here were performed in the $\theta = 0°$ plane located midway between two baffles, with all three velocity components being measured with the beams entering either through the base or sidewalls of the vessel, except for the $\overline{W}$ and w' measurements in the 294-mm vessel, which were obtained by orientating the beams at $\pm 45°$ to the θ-direction, in the manner described by Yianneskis et al. (1987). The position of the LDA measuring volume and the change in the beam angle due to refraction at the vessel walls was determined for each measurement location in coordinates relative to the vessel axis using an iterative computer program. Extensive checks were made to minimize the positional error through careful alignment with respect to the impeller-blade tip, and the entire optical system was mounted on a traversing mechanism that allowed the measuring volume to be located within the vessel with an accuracy of 0.05 mm in the r and θ directions and 0.1 mm in the z-direction. In general the errors in the mean velocities were estimated to be approximately 1% of the blade-tip velocity (V_{tip}), rising to 2–3% in regions of steep velocity gradients, while the errors in the measured turbulent fluctuations are in the region of 5–10%.

Experimental Results and Discussion

The flow visualization experiments showed that the clearance of the lower impeller from the base of the mixing vessel ($C1$), the separation between the impellers ($C2$), the submergence of the upper impeller below the fluid free surface ($C3$), and the liquid column height (H) (see Figure 2) strongly affected the overall flow structure in the vessel.

Three stable flow patterns were observed during the flow visualization experiments with different lower impeller clearance ($C1$), impeller separation ($C2$), and upper impeller submergence ($C3$) values and are shown in Figure 3. The so-called "parallel flow" pattern of Figure 3a was observed with an impeller clearance equal to $0.25T$, impeller separation $0.50T$, and upper impeller submergence of $0.25T$. It can be seen that the Rushton impellers operate essentially independently of one another with this configuration, each impeller producing its own characteristic upper and lower ring vortex leading to the formation of four stable ring vortices. In order to maintain this flow pattern it was found that $C1$ must be greater than $0.20T$, and $C2$ must be greater than $0.385T$. Hence, a $C3$ value of less than $0.415T$ is required to generate this flow pattern.

When the impeller clearance and separation were each set equal to $T/3$, the flow pattern of Figure 3b was produced. In this case the C1 value must be kept above $0.17T$ and $C2$ must be less than $0.385T$. This was termed "merging flow" since the impeller streams follow an almost straight-line orientation toward one another, and merge at an elevation midway between the impellers to form two large ring vortices. A similar flow structure has been reported in gassed mixing vessels by Kuboi and Nienow (1982).

The third of the stable flow patterns was termed "diverging flow" since as a result of the low position of the lower Rushton impeller the impeller stream follows a path toward and impinges upon the base of the vessel, as shown in Figure 3c. This resulted in the lower Rushton impeller producing one large ring vortex, while the upper Rushton impeller produced two well-defined ring vortices above and below the impeller disk. The diverging flow was observed with $C1 = 0.15T$,

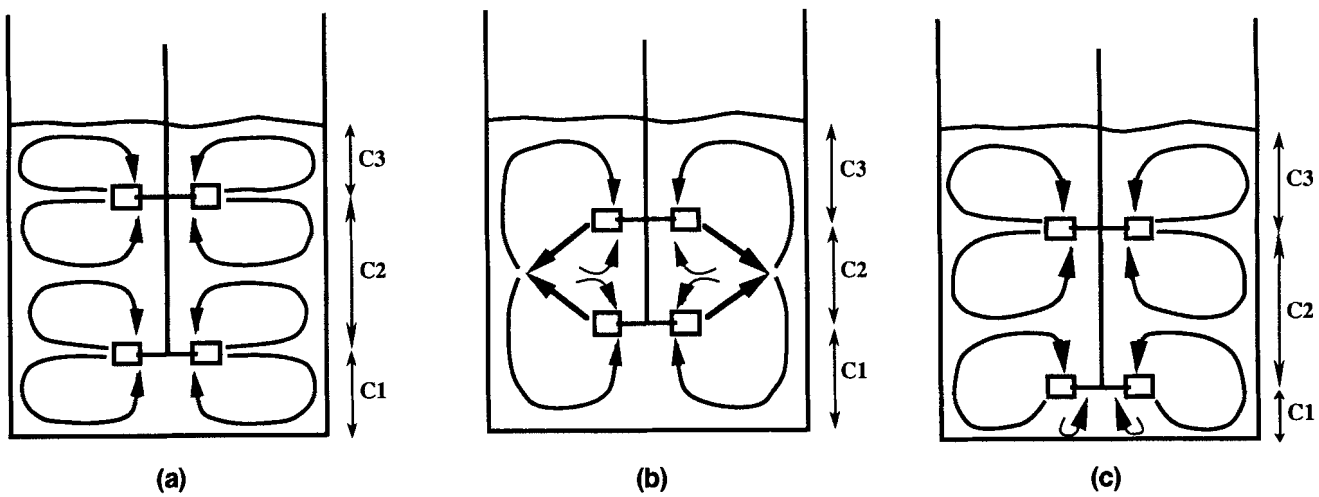

Figure 3. Stable flow patterns obtained in a dual-Rushton turbine stirred vessel.
(a) Parallel flow; (b) merging flow; (c) diverging flow.

$C2 = 0.50T$, and $C3 = 0.35T$. This flow pattern was maintained so long as the separation $C2$ was greater than $0.385T$ and the lower impeller clearance $C1$ was less than $0.15T$.

Combinations of $C1$ and $C2$ values other than those mentioned earlier resulted in unstable flow patterns alternating between any two or all three of the parallel, merging, and diverging regimes.

Power number, mixing time, and Flow number

Torque measurements were performed for all stable dual-Rushton impeller configurations for a range of impeller rotational speeds between $N = 100$ and 250 rpm in the 294-mm-diameter vessel. It was found that the mean value of the Power numbers varied little with impeller speed. At the impeller speed used in the present investigation ($N = 250$ rpm), the highest total Power number (for both impellers) was obtained with the parallel flow configuration ($Po = 10.0$), the diverging flow pattern had a slightly lower Power number ($Po = 9.5$), while the merging flow configuration yielded the lowest value ($Po = 8.4$). For comparison purposes, the corresponding Power number measured with a single Rushton impeller of the same thickness, when an impeller clearance of $T/3$ from the vessel base and a liquid column height $H = T$ was employed, was 5.4.

Mixing time measurements carried out using a conductivity probe technique described in detail by Mahmoudi (1994) showed the merging flow led to a mixing time lower by around 20% compared to the parallel and diverging flow patterns, and that unstable flow patterns generally had the highest mixing time values associated with them.

The ensemble-averaged radial mean velocity profiles near the impeller tip at $r/T = 0.173$ were used to calculate the Flow number Fl, from the 360° ensemble-averaged mean velocity profile using relationships 1 and 2 below where Q is the impeller pumping capacity, $\bar{V}$ is the radial mean velocity component, r and z are the radial and axial coordinates of the measurement locations, and the integration limits h^* and $-h^*$ are defined as the points above and below the impeller disk, respectively, where the radial mean velocity reaches zero:

$$Q = \int_{-h^*}^{h^*} 2\pi r \bar{V} dz \tag{1}$$

$$Fl = \frac{Q}{ND^3}. \tag{2}$$

It was not practical to calculate Fl for the merging and diverging flow patterns accurately due to the inclination of the impeller streams. However, with the parallel flow pattern, Fl for the upper impeller was 0.79, slightly higher than that for the lower impeller (0.76). These Flow numbers compare well with those obtained for single Rushton impellers with T/2 clearance by Cooper and Woolf (1968) and Stoots and Calabrese (1994) and with $T/3$ clearance by Yianneskis et al. (1987), which were 0.8, 0.75, and 0.785, respectively, and are within the limits of $Fl = 0.75 \pm 0.15$ for single Rushton impellers recommended by Revill (1982). However, it is difficult to distinguish between differences in Fl due to the variation in the impeller configuration from those associated with the location and extent of the integrated radial velocity profiles of previous studies.

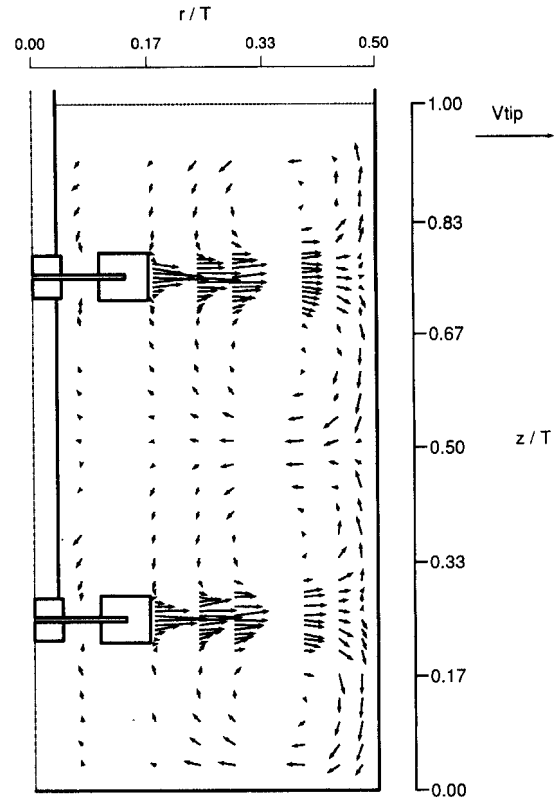

Figure 4. Parallel flow $\theta = 0°$ r-z plane 360° ensemble-averaged mean velocity vectors: ($C1 = 0.25T$, $C2 = 0.50T$).

Ensemble-averaged mean velocity vectors

Characteristic mean velocity vectors in the r-z plane are presented in Figures 4 to 6 for the parallel, merging and diverging flow patterns, respectively. The vectors were plotted from 360° ensemble-averaged LDA measurements of the axial and radial velocity components obtained in the $\theta = 0°$ plane midway between two baffles in the $T = 294$ mm vessel, and normalized with respect to the impeller-blade-tip velocity (V_{tip}). The vector plots presented show the main flow features and structures such as the orientation of the impeller discharge stream and the ring vortices formed above and below the impeller discs.

The parallel flow velocity vectors of Figure 4 clearly show the presence of the four ring vortices described previously, one above the upper Rushton impeller, two between the impellers, and one below the lower impeller. The highest velocities were, of course, measured near the blade tip. The impeller streams are directed toward the vessel wall at a small angle (3°–5°) to the horizontal, and the velocities in the rest of the vessel are small in comparison with those in the impeller streams.

In contrast, with the merging flow arrangement (Figure 5), the impeller streams are clearly inclined toward one another and follow an essentially straight-line path until they merge at an elevation approximately midway between the impellers.

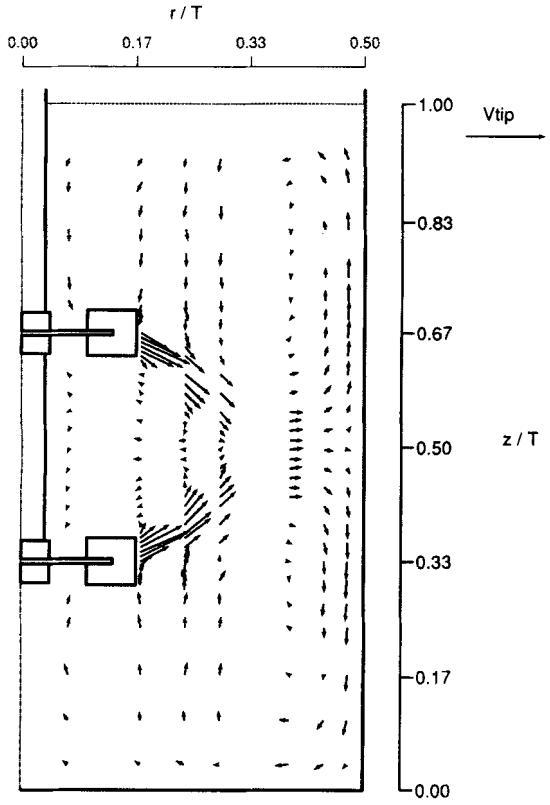

Figure 5. Merging flow $\theta = 0°$ r-z plane 360° ensemble-averaged mean velocity vectors: ($C1 = 0.33T$, $C2 = 0.33T$).

The two large ring vortices observed during the flow visualization experiments can be seen in the vector plot, and again the velocities are much larger in the impeller stream region than in the vessel bulk flow. However, the normalized velocities are generally smaller in the merging flow impeller stream than was the case with the parallel flow configuration.

The most striking feature of the vectors plotted in Figure 6 for the diverging flow pattern is the orientation of the discharge stream of the lower impeller toward the vessel base. Again the highest velocities are found in the impeller stream that impinges upon the vessel base to form the single-ring vortex shown. The flow generated by the upper impeller seems to be unaffected by the presence of the lower impeller since the upper impeller stream is directed horizontally toward the vessel wall, where it impinges to form two ring vortices. These vortices are similar to, but larger than, those found in the parallel flow. Marginally higher velocities than in parallel flow are found in the upper impeller stream of the diverging flow. Fluid is entrained into the upper Rushton impeller stream at both the top and bottom edges of the impeller stream, while entrainment into the lower impeller stream occurs primarily from the upper edge of the lower impeller blades due to the influence of the large ring vortex.

Ensemble-averaged turbulence kinetic energy distributions

Contour plots of the turbulence kinetic energy, $k = \frac{1}{2}(u'^2 + v'^2 + w'^2)$, normalized using the impeller-blade-tip velocity, (k/V_{tip}^2), are presented in Figures 7, 8, and 9 for the parallel, merging and diverging flow patterns, respectively. As with the velocity vectors plotted in Figures 4 to 6, these contours were obtained from 360° ensemble-averaged LDA measurements of the axial, radial and tangential velocity components performed in the $\theta = 0°$ plane in the 294-mm-diameter vessel. From these figures a direct comparison of the levels of turbulence kinetic energy generated with the three flow patterns can be made. The orientation and strength of the impeller discharge streams are indicated by the highest turbulence levels (above 0.04 V_{tip}^2) present in the impeller stream region for all three flow patterns, which indicate the occurrence of vigorous mixing in these regions.

For the parallel flow pattern (Figure 7), it can be seen that the lowest turbulence levels, up to 0.02 V_{tip}^2, are found in the vicinity of the vessel wall, near the base of the vessel, and close to the free surface of the liquid. In these regions the turbulent kinetic energy is at least eight times lower than the levels found in the vicinity of the rotating impellers. As expected from the vector plot for this flow pattern, shown in Figure 4, the impeller streams are both directed horizontally toward the vessel wall. In general, it was found that in the vessel bulk flow, that is, in regions away from the impeller streams, the parallel flow pattern resulted in the steepest gradients of turbulence kinetic energy, with the diverging flow pattern producing the smallest variation.

Comparing Figures 7 to 9, the merging flow pattern can be seen to generate turbulence levels in the vessel bulk flow that are typically 30% lower than those generated by the parallel flow pattern, while the diverging flow produced the lowest

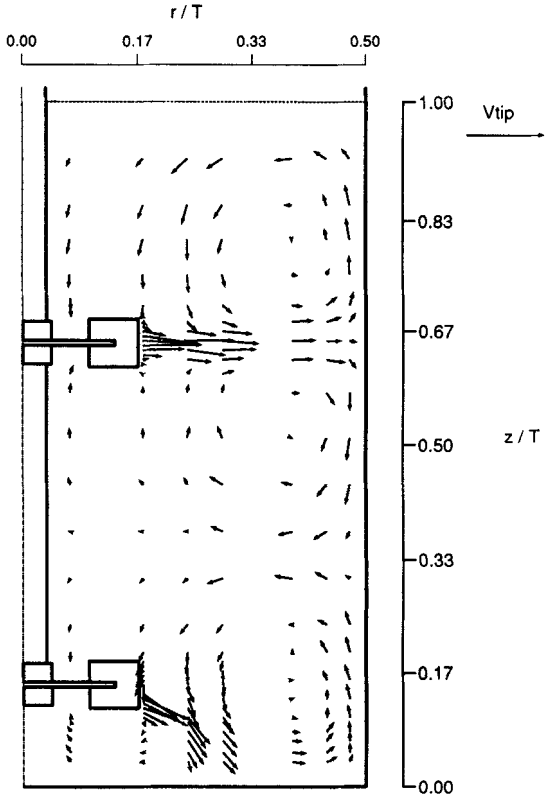

Figure 6. Diverging flow $\theta = 0°$ r-z plane 360° ensemble-averaged mean velocity vectors: ($C1 = 0.15T$, $C2 = 0.50T$).

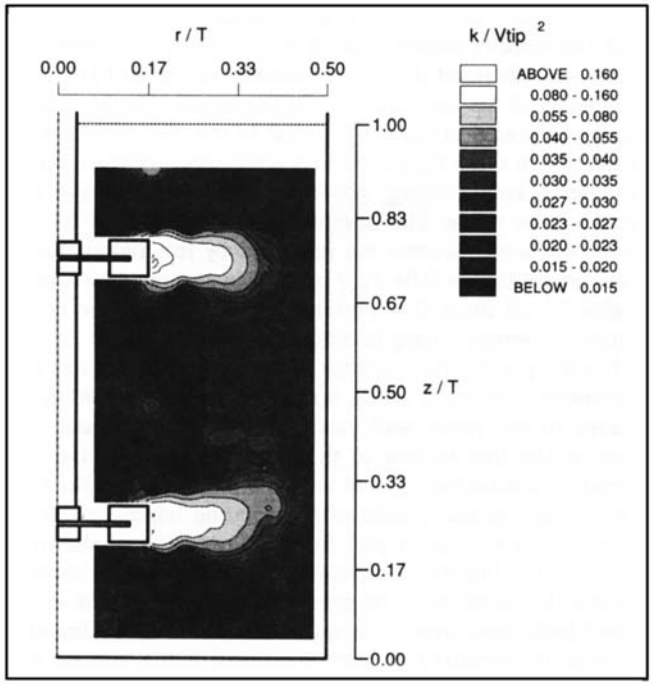

Figure 7. Parallel flow $\theta = 0°$ r-z plane 360° ensemble-averaged contours of kinetic energy of turbulence.

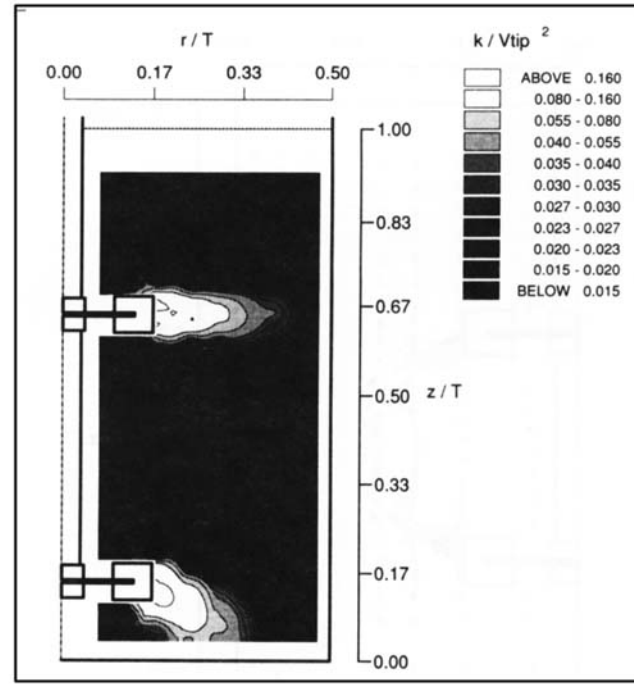

Figure 9. Diverging flow $\theta = 0°$ r-z plane 360° ensemble-averaged contours of kinetic energy of turbulence.

turbulence levels in regions away from the impeller streams. Steep gradients of turbulent kinetic energy are found over the entire region between the impellers in Figure 8 for the merging flow pattern. As a consequence of the downward inclination of the lower impeller stream, the diverging flow pattern produced the highest turbulence levels beneath the lower impeller, while the lowest turbulence levels were produced in this region by the merging flow pattern.

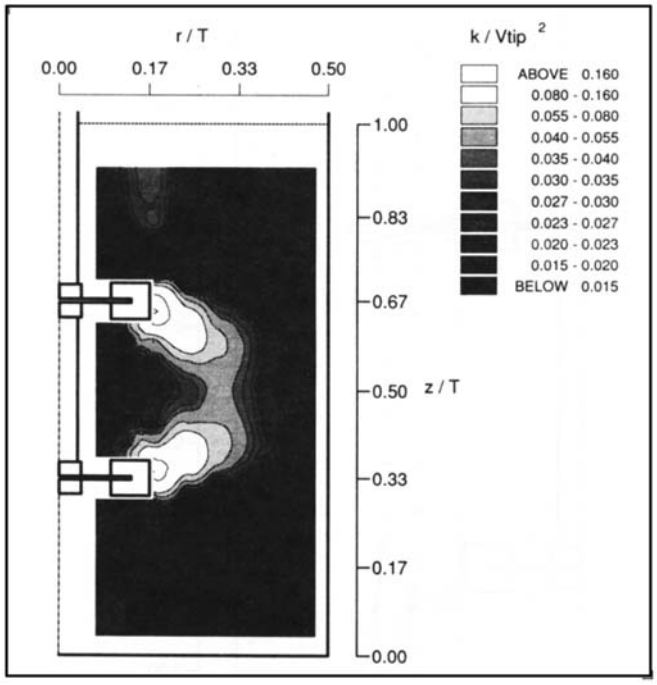

Figure 8. Merging flow $\theta = 0°$ r-z plane 360° ensemble-averaged contours of kinetic energy of turbulence.

The most uniform distribution of high levels of k throughout the vessel was obtained with the parallel flow pattern. However, in the upper part of the vessel close to the liquid free surface the merging flow pattern produced the highest levels of k, even though the parallel flow pattern had the highest positioning of the upper impeller. A possible explanation for the region of higher k above the upper Rushton impeller in Figure 8 is the presence of a precessing free vortex around the impeller shaft, which has been described by Yianneskis et al. (1987).

The 360° ensemble-averaged velocity vectors and turbulence level plots presented indicate that varying the impeller separation and clearance in dual-impeller configurations can lead to a significant alteration in the local macromixing and micromixing characteristics. The three flow patterns provide potentially useful mean flow and turbulence distributions: parallel flow to achieve higher turbulence levels and more uniform blending in the bulk of the vessel away from the impeller streams, merging flow for locally intensive mixing in the middle of the vessel, and diverging flow for suspension of solids deposited on the bottom of the vessel. However, the merging flow pattern should be preferable for overall blending performance, due to the 20% lower mixing time recorded for this configuration.

Ensemble-averaged rms velocity distributions

Since the merging flow pattern led to the lowest power consumption and mixing time of the three stable flow config-

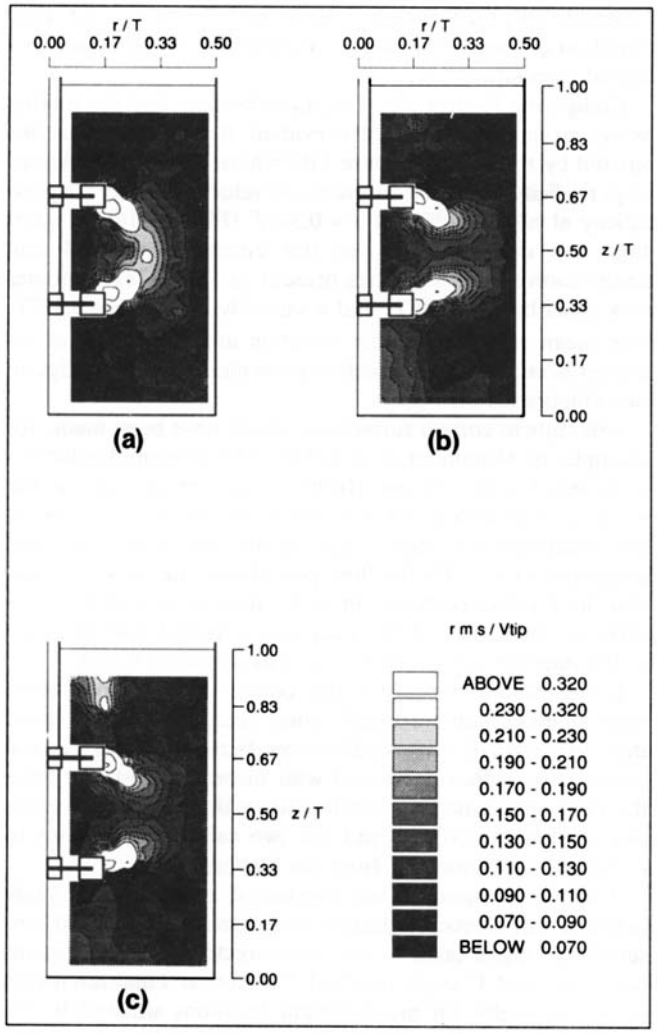

Figure 10. Merging flow $\theta = 0°$ r-z plane 360° ensemble-averaged rms velocity contours.

(a) Axial. (b) Radial. (c) Tangential.

urations, it was selected for further investigation. The axial, radial, and tangential rms velocity components (u'/V_{tip}, v'/V_{tip}, w'/V_{tip}) are shown in normalized contour form in Figures 10a to 10c, respectively. As with the velocity vectors and contours of k already presented, these contours were plotted from 360° ensemble-averaged LDA data obtained in the $\theta = 0°$ plane.

High turbulence levels are found in the impeller stream region, and the inclination of the impeller stream observed for the merging flow pattern in Figure 8 is evident in all three rms velocity distributions. In the vicinity of the impellers rms levels exceeding 0.320 V_{tip} are generated in the impeller stream. It can be seen that the radial and tangential rms velocity components have similar values, between 0.13 and 0.15 V_{tip} at the point where the upper and lower impeller streams merge, while the axial values at this location are significantly higher, around 0.21–0.23 V_{tip}.

The bulk flow radial and tangential rms velocity distributions display a number of similarities such as relatively high values (0.11–0.13 V_{tip}) in the vicinity of the impeller shaft, while lower values are found close to the vessel wall (0.07–0.09 V_{tip}). The opposite trend is found with the axial rms velocity, which displays significantly lower values in the vicinity of the impeller shaft than either the radial or tangential components. Below the lower impeller the radial rms velocity was found to be the highest, with the axial rms velocity being the lowest. Differences are also evident in the rms velocities in the region between the impellers. The presence of the local area of higher k evident near the fluid surface in Figure 8 is also evident in the tangential rms velocity distribution of Figure 10c, as might be expected since the free surface vortex is likely to have a strong tangential (swirl) velocity.

The rms velocity contour plots presented indicate that the turbulence structure in the stirred vessel is in general anisotropic, especially in the vicinity of the rotating impellers, in agreement with the findings of Yianneskis et al. (1987) for the flow generated by a single Rushton impeller. This observation can have important consequences for CFD flow predictions that employ the standard k-ϵ model to represent the turbulent processes. The formulation of the model makes use of the same eddy viscosity ν_t for the three components of the Reynolds stress, that is u', v', and w', and therefore there is an implicit assumption of locally isotropic turbulence (Abbot and Basco, 1989). As the data clearly show that u', v', and w' can vary significantly in parts of the flow, the use of Reynolds stress turbulence models that do not assume local isotropy might be expected to yield more accurate predictions.

Comparison of ensemble-averaged and angle-resolved measurements

It has been previously stated that although 360° ensemble-averaged LDA measurements can provide useful information on the overall flow structure and levels of turbulence in a stirred vessel, such measurements cannot account for the variation in the mean velocity resulting from the passage of the impeller blades and the associated trailing vortices. In order to assess the effect of this, 1° angle-resolved LDA measurements, which show the periodic variation of the mean velocity, are compared with 360° ensemble-averaged LDA measurements in Figure 11 for the merging flow configuration. The results were obtained at three radial locations: $r = 0.178T$, $r = 0.218T$, and $r = 0.347T$, and an elevation $z = 0.33T$ corresponding to the midsection of the lower Rushton impeller. These positions were chosen so that the first one was located in the middle, the second near the boundary, and the third outside the inclined impeller stream.

The 1° angle-resolved mean velocity variation shown in Figure 11a shows clear evidence of the trailing vortex structure in the vicinity of the impeller blade, since the change in sign of the radial mean velocity is indicative of the presence of the vortex (Yianneskis and Whitelaw, 1993). The ensemble-averaged mean velocity at this location, indicated by the lower dashed line, clearly does not account for the strong periodic nature of the flow, as $\bar{V}$ varies from around 0.8 m/s near the leading blade ($\phi < 10°$) to around 0.1 m/s at $\phi \approx 40°$.

Ensemble-averaging over 360° leads to an overestimation of the rms velocity in comparison with the 1° angle-resolved rms values over part of the 60° interval. Near the leading and trailing blades (Figure 11a), the ensemble-averaged and an-

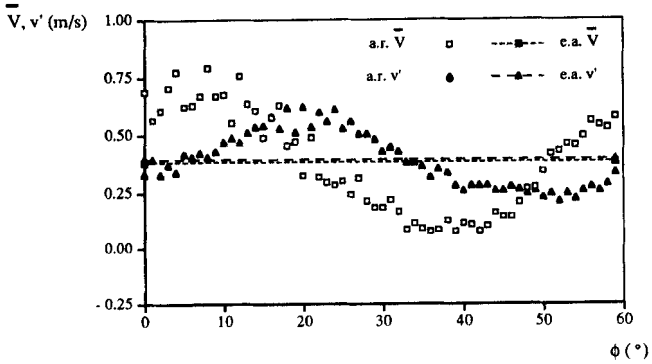

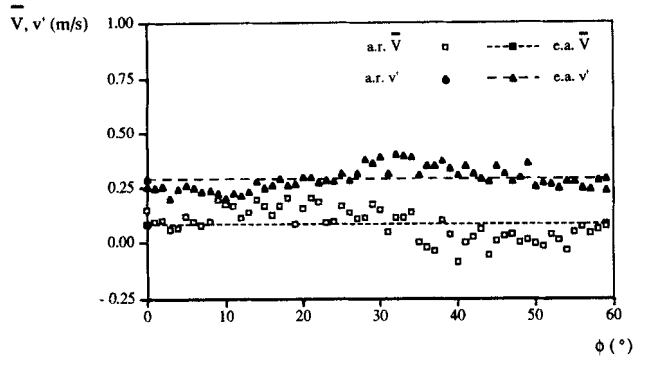

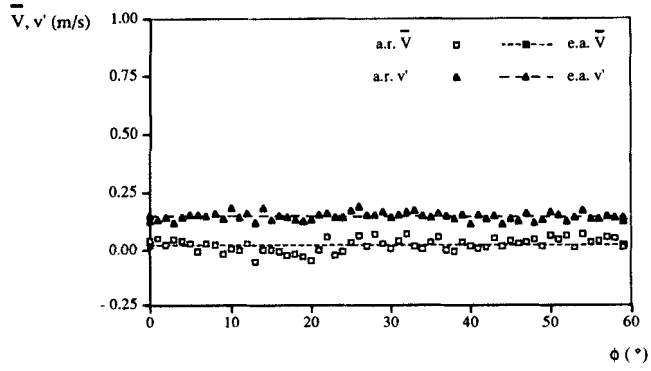

Figure 11. Comparison of 1° angle-resolved mean and rms radial velocity variations with 360° ensemble-averaged mean and rms radial velocities for a dual-Rushton merging flow configuration in the $T = 294$ mm vessel.

(a) $r = 0.178T$, $z = 0.33T$. (b) $r = 0.218T$, $z = 0.33T$. (c) $r = 0.347T$, $z = 0.33T$.

gle-resolved v' values are similar, but elsewhere they vary significantly: the angle-resolved values are around 70% higher at $\phi = 20°$ and 70% lower at $\phi = 50°$. It must be noted that in some locations in the impeller stream differences were larger, with ensemble-averaged values up to four times the angle-resolved ones, in agreement with the findings of Yianneskis and Whitelaw (1993). This overestimation of the turbulence levels is attributed to the influence of the blade passages and associated trailing vortices at this location, as 360° ensemble-averaged measurements include the mean flow variation or pseudoturbulence, in addition to the actual turbulent fluctuations.

Comparing Figures 11a–11c, it can be seen that the trailing vortex structure that is clearly evident at $r = 0.178T$ has dissipated by $r = 0.218T$ (Figure 11b) where only a small degree of periodicity is present in the mean velocity profile. No periodicity at all is evident at $r = 0.347T$ (Figure 11c). In addition, the disparity between the ensemble-averaged and angle-resolved rms velocities present at $r = 0.178T$ becomes very small by $r = 0.218T$, and is virtually zero by $r = 0.347T$. The mean velocities at this elevation are very small, as expected from the velocity vectors presented for this configuration (Figure 5).

Attempts to correct turbulence values have been made, for example, by Mujumdar et al. (1970), who measured velocities in a vessel with a single Rushton impeller and air as the working fluid with a hot-wire anemometer. An autocorrelation technique was used to correct the measured turbulence intensities ($I = v'/\bar{V}$) for flow periodicity, and it was stated that the I values corrected in such a manner provided a more accurate indication of the microscopic turbulence structure in the impeller stream region than uncorrected values.

In the impeller vicinity a large correction was shown to be implemented, with corrected values being consistently lower than uncorrected ones. Differences between corrected and uncorrected values decreased with increasing distance from the blade tip, which was attributed to the associated reduction in flow periodicity, and the two values were shown to converge at locations far from the blades.

A similar comparison was conducted in the present study between turbulence intensities calculated from the 360° ensemble-averaged (akin to the "uncorrected" data of Mujumdar et al.) and 1° angle resolved ("corrected") measurements at two ϕ angles for measurement locations situated in the impeller stream. The results are presented in Figure 12. Due to the inclination of the impeller stream, I values are plotted against d, the distance from the midsection of the lower impeller tip along the inclined stream, that is,

$$d = \sqrt{(r - r_0)^2 + (z - z_0)^2}, \tag{3}$$

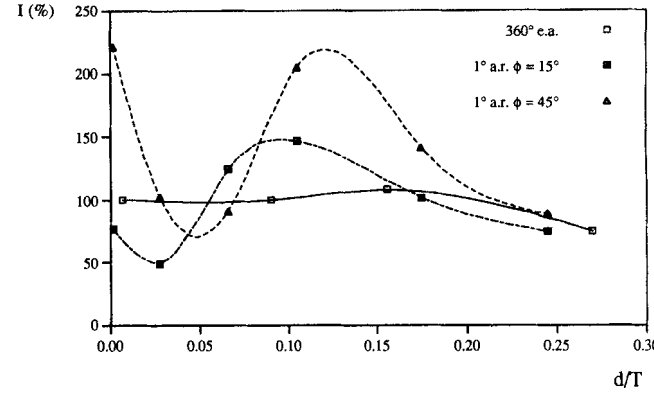

Figure 12. Comparison of relative turbulence intensities calculated from 360° ensemble-averaged and 1° angle-resolved LDA measurements in the impeller stream region.

where r and z are the radial and axial coordinates of the measurement location in the inclined impeller stream, and r_0 and z_0 are the coordinates of the middle of the lower impeller blade tip, that is, $r_0 = 0.165T$ and $z_0 = 0.33T$.

It can be seen that in contrast with the findings of Mujumdar et al., the data that show the periodic variation of the mean velocity (1° angle resolved) are not always lower than those that do not show this variation (360° ensemble-averaged). The angle-resolved turbulence intensity variations are similar in character for both of the ϕ angles presented; however, the variation of I is larger for $\phi = 45°$. The data indicate clearly that it may not be appropriate to correct measurements for the effect of flow periodicity in the manner suggested by Mujumdar et al..

At around $d/T = 0.20–0.30$ the three sets of results are very similar, indicating that the periodicity has decayed almost entirely. The single Rushton impeller work of Stoots and Calabrese (1994) showed the periodicity of the mean flow to decay with increasing distance from the impeller, dissipating entirely at radii larger than $0.85D$, that is, $0.35D$ from the blade tip. The present results (both the turbulence intensity profiles of Figure 12 and the corresponding mean velocity variations that are not presented here) indicate that the periodicity in the inclined impeller stream turbulence intensity dissipates after around $0.2T$ ($0.6D$) from the blade tip. This difference with the single impeller findings may be due to the stronger rotational flow induced by the two-impeller system, resulting in the periodic structures maintaining their identity in the inclined impeller stream longer. However, as will be shown below, the trailing vortex axis is more curved due to the stronger rotation and as a result the periodicity is contained within a smaller radius in the merging flow configuration.

Although other periodic motions occur in stirred vessels that may result in the obvious differences between the 1° angle-resolved and 360° ensemble-averaged mean and rms velocity distributions, such as the free surface vortex precessing around the impeller shaft, the blade crossings and associated trailing vortices might be expected to be the main reason for these differences.

Predictions of the flow that treat the impeller as a rotating disk, rather than as individual rotating blades, can only be assessed against ensemble-averaged data, as the variation of velocities and turbulence levels with ϕ near the impeller is not accounted for. However, as ensemble-averaged turbulence level data also include the variation in the mean velocity with impeller revolution, predicted k values will invariably be lower than measured ones, as this variation is not included in the modeling. Therefore, the accuracy of such predictions in regions away from the impeller can be improved if the impeller region is excluded from the calculation. This region where flow periodicity is dominant is defined in the penultimate section below.

Angle-resolved mean velocity vectors and scaling effects

In order to characterize the effect of vessel size on the flow and turbulence characteristics of a stirred vessel operating with two Rushton impellers arranged in the merging flow configuration, 1° angle-resolved LDA measurements were performed in both vessels ($T = 100$ mm and $T = 294$ mm). Figure 13 shows the flow structure measured around the lower

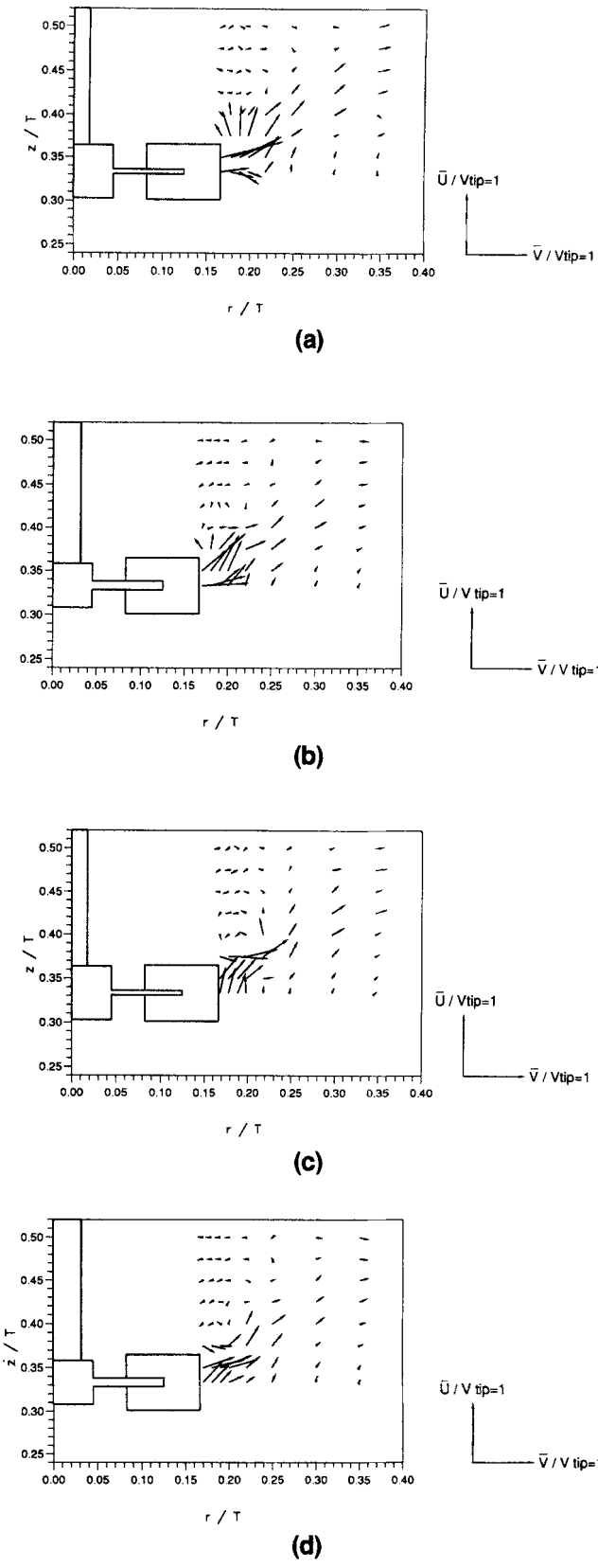

Figure 13. Comparison of the $\theta = 0°$ r-z plane 1° angle-resolved velocity vectors in the vessels studied.

(a) $T = 294$ mm, $\phi = 15°$, (b) $T = 100$ mm, $\phi = 15°$, (c) $T = 294$ mm, $\phi = 45°$, (d) $T = 100$ mm, $\phi = 45°$.

impeller within an area extending radially from the lower impeller tip to $r = 0.35T$, and axially from the midsection of the lower impeller disk to an elevation midway between the impellers. These vectors were plotted from 1° angle-resolved LDA measurements of the axial and radial velocity components normalized with V_{tip}, and are shown for each vessel in Figure 13 in the r-z planes at $\phi = 15°$ and $\phi = 45°$ behind the leading blade.

By comparing Figures 13a and 13b for $\phi = 15°$ in the T = 294-mm and 100-mm vessels respectively, it can be seen that the flowfields are generally similar. Both the flow due to the blade passage and the inclination of the impeller discharge flow at approximately 45° to the horizontal can be identified. These features can also be seen in Figures 13c and 13d for $\phi = 45°$. The development of the flow with blade angle can also be observed in Figure 13, especially in the vicinity of the blade tip where the trailing vortex is evident in Figures 13c and 13d. It should be noted that at $\phi = 15°$ some of the vectors close to the impeller tip are almost vertical, due to the proximity of the center of the trailing vortex to the impeller blade tip at this ϕ angle. As ϕ increases, the vortex strength is reduced and its center is displaced radially and axially away from the impeller tip.

In general, agreement between the normalized velocity vectors in the two vessels is good, since the main flow features are essentially the same and the center of the trailing vortex is located at approximately $z = 0.39T$ at $\phi = 45°$ in both instances. Also, the inclination and strength of the impeller stream is similar in both vessels, although differences in the direction of the impeller stream can be observed in the immediate vicinity of the blade. van der Molen and van Maanen (1978) reported an increase in normalized velocity with vessel size in vessels of similar diameter to those used in the present study. In the results presented here, the normalized velocity vectors are slightly larger for the 294-mm vessel; this has been established, however, to be due to the smaller thickness of the impeller used in the larger vessel (Rutherford et al., 1995) and it is not likely to be related to the vessel size.

Trailing vortex axis

The location of the mean axis of the trailing vortex generated by the lower Rushton impeller is plotted in Figure 14. This figure shows the axis in the r-θ plane as viewed from above the tank, with the impeller rotating in a clockwise direction as indicated. For comparative purposes the trailing vortex axes determined previously by van't Riet et al. (1975), Yianneskis et al. (1987), and Stoots and Calabrese (1994) for single Rushton impeller configurations are also shown.

van't Riet et al. utilized a photographic technique to find the location of the axis by determining the locations where a velocity component perpendicular to the axis was zero. Since the axis of the trailing vortex was reported to be essentially horizontal for a single Rushton impeller system, the axial velocity component was most suitable. It should be noted, however, that Stoots and Calabrese (1994) found the axis of the trailing vortex to be 8° to 10° to the horizontal. The investigations of Yianneskis et al. and Stoots and Calabrese determined the vortex axis from angle-resolved LDA mean velocity data. The discrepancies between the vortex axis presented

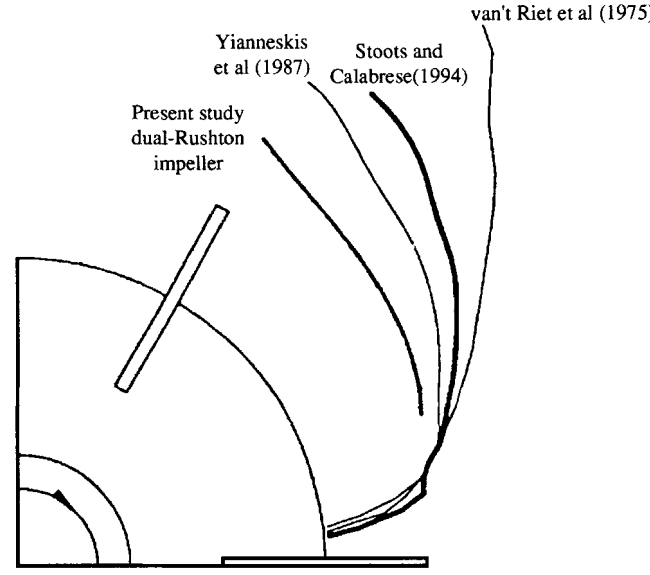

Figure 14. Comparison of the axis of the trailing vortex shed from the lower impeller in a dual-Rushton merging flow configuration with that for a single Rushton configuration, as viewed from above the vessel in the r-θ plane (clockwise impeller rotation).

in these three investigations were attributed by Stoots and Calabrese to differences between various system characteristics, such as the impeller geometry, the clearance of the impeller from the base of the vessel, and the impeller rotational speed.

The vortex axis for the present study was also determined from the locations where the mean axial velocity component was zero. This was employed as an approximation since it is not possible to determine the velocity component that is zero in a plane perpendicular to the axis of the trailing vortex, due to the inclination of the impeller streams. It can be seen from Figure 14 that the center of the trailing vortex produced by the lower Rushton impeller does not extend as far into the vessel as for a single impeller configuration. The vortex axis presented by Yianneskis et al. extended to $r = 0.23T$ (ϕ = 60°), while with the dual impeller configuration of the vortex center only extends to $r = 0.195T$ ($\phi = 55°$); this is attributed to the stronger rotational velocities and the impeller stream inclination, as mentioned earlier.

Angle-resolved turbulence level and kinetic energy distributions

Characteristic r-z plane contours of radial rms velocity obtained from 1° angle-resolved LDA measurements performed in the T = 294-mm and 100-mm vessels are presented in Figure 15. The 1° angle-resolved LDA data obtained in the T = 100-mm vessel was used to plot the contours of turbulent kinetic energy shown in Figure 16. As in Figure 13, these figures show the flow structure around the lower impeller, in this case for ϕ ranging from 0° to 45°. All v' and k values have again been normalized with V_{tip} and V_{tip}^2, respectively.

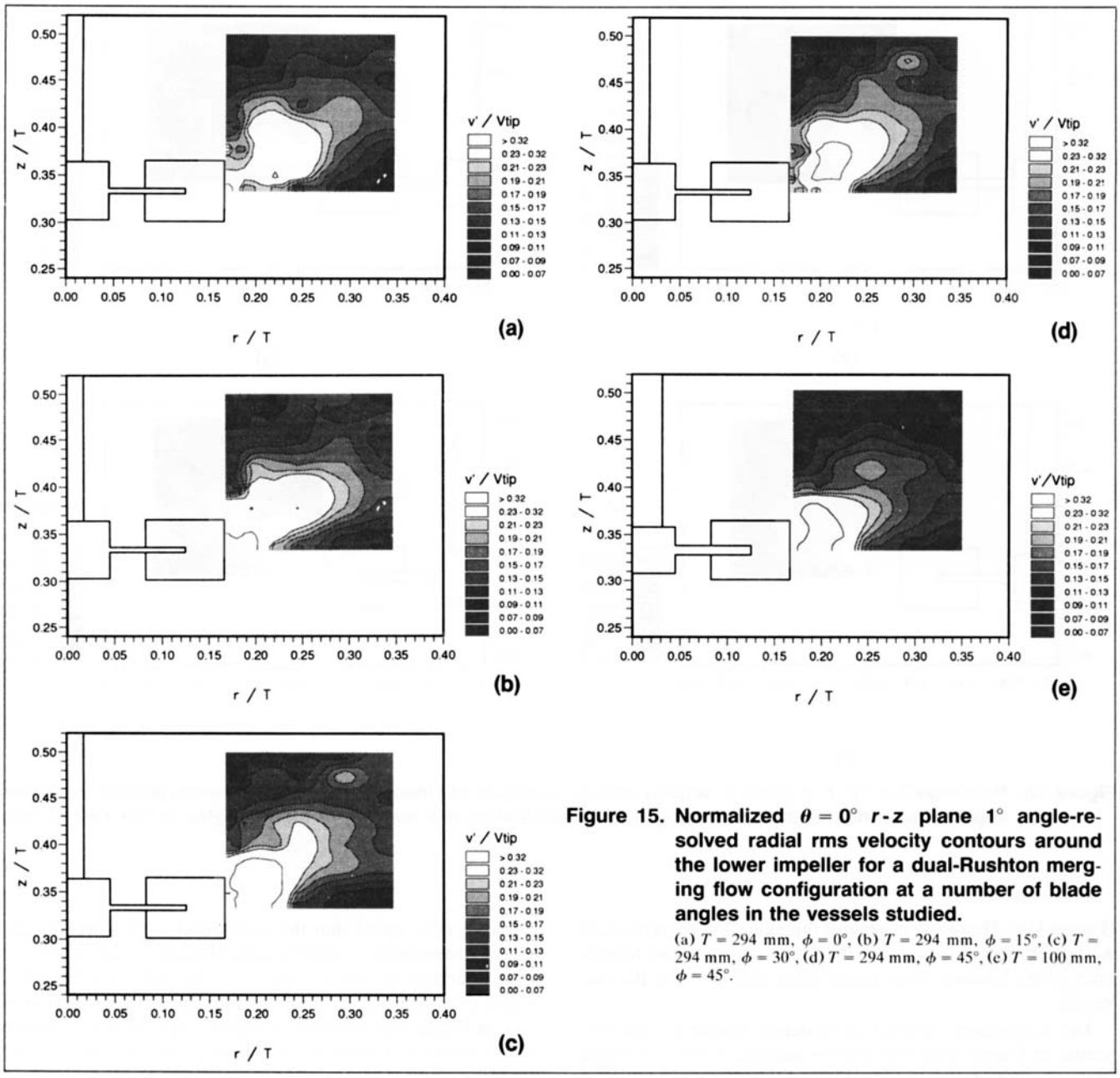

Figure 15. Normalized $\theta = 0°$ r-z plane 1° angle-resolved radial rms velocity contours around the lower impeller for a dual-Rushton merging flow configuration at a number of blade angles in the vessels studied.

(a) $T = 294$ mm, $\phi = 0°$, (b) $T = 294$ mm, $\phi = 15°$, (c) $T = 294$ mm, $\phi = 30°$, (d) $T = 294$ mm, $\phi = 45°$, (e) $T = 100$ mm, $\phi = 45°$.

Comparing Figures 15a–15d the formation and development of the trailing vortex is indicated by the region of the highest rms velocity level (greater than 0.32 V_{tip}) expanding in area and moving radially and axially away from the center of the impeller tip with increasing ϕ. In Figure 15a ($\phi = 0°$), this region is small, approximately $0.005T$ in diameter, and located between the impeller tip and $0.175T$ at the impeller midsection elevation, while by $\phi = 45°$ (Figure 15d) it is approximately $0.04T$ in diameter, and is situated between $r = 0.19T$ and $0.23T$ radially and $z = 0.35T$ and $0.39T$ axially. It must be noted that the near-circular region of 0.23–0.32 level in Figure 15a centered around $r/T = 0.23$ is associated with the trailing vortex generated by the preceding blade.

In the results presented the region of highest rms velocities is largest in Figure 15c for the impeller blade angle $\phi = 30°$. The equivalent 360° ensemble-averaged contours presented in Figure 10b show the region of highest rms velocities to extend into the vessel from the impeller tip to approximately $0.22T$ radially, in contrast with the contours presented in Figures 15a–15d which show the outer extent of this region to vary between $0.175T$ ($\phi = 0°$) and $0.23T$ ($\phi = 45°$). The orientation of the impeller stream at approximately 45° to the horizontal is again evident in Figures 15a–15d, in good agreement with the 360° ensemble-averaged results.

The r-z plane contours of v'/V_{tip} at $\phi = 45°$ are shown in Figure 15e for the $T = 100$-mm vessel. Comparison of Figures 15d and 15e shows that the turbulence distributions in the two vessels display similar characteristics. The rms velocity levels are generally similar in both vessels, although there is some discrepancy between the locations and magnitude of the regions of highest rms velocity. The maximum value can be seen to extend over a larger area in the $T = 100$-mm vessel

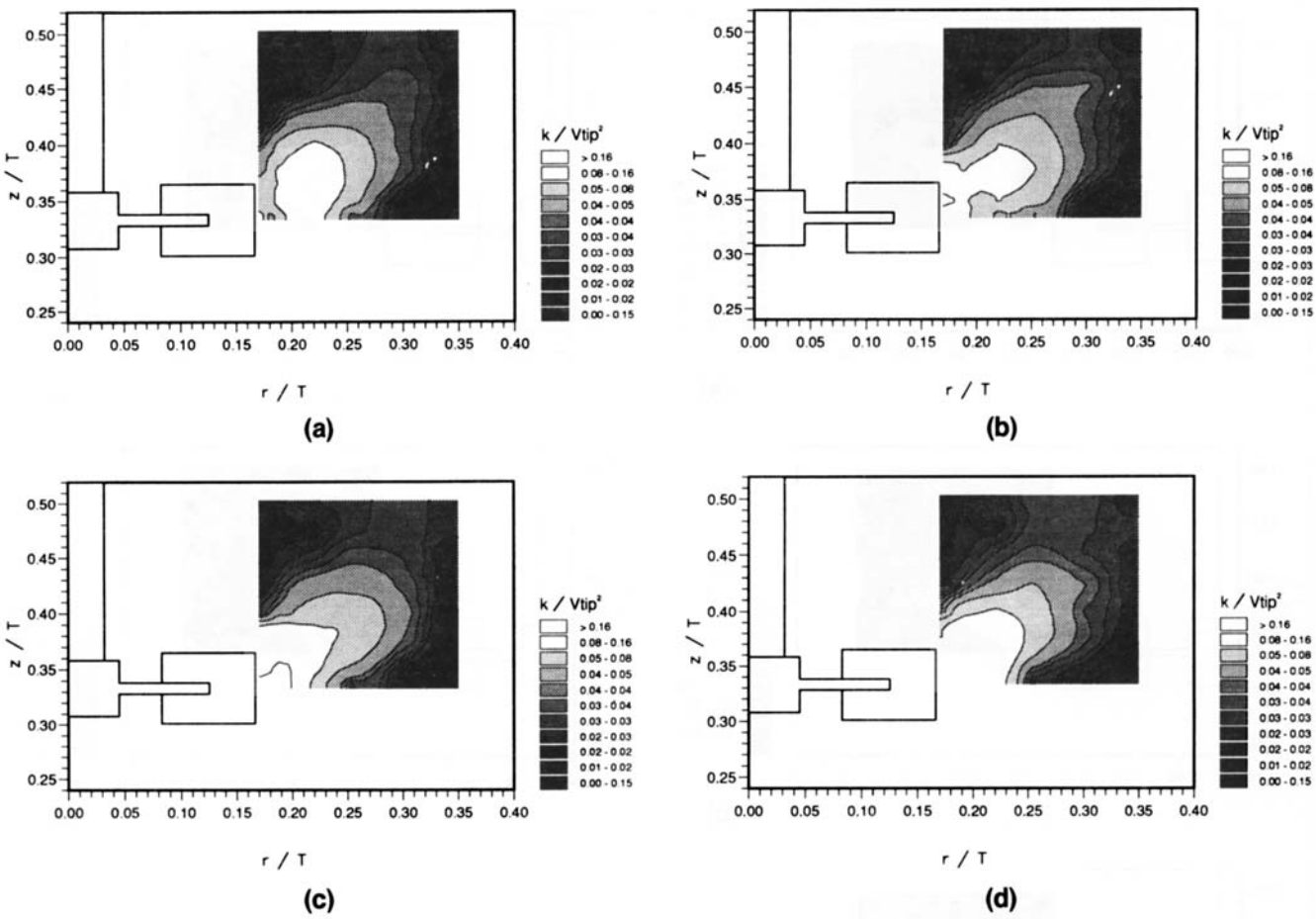

Figure 16. Normalized $\theta = 0°$ r-z plane 1° angle-resolved contours of kinetic energy of turbulence around the lower impeller for a dual-Rushton merging flow configuration at a number of blade angles in the $T = 100$ mm vessel.

(a) $\phi = 0°$, (b) $\phi = 15°$, (c) $\phi = 30°$, (d) $\phi = 45°$.

(Figure 15e). However, in general the main flow features such as the turbulence levels near the blade and near the boundaries of the measurement region scale well between the two vessels.

The normalized contours of turbulent kinetic energy presented in Figures 16a–16d for the measurements performed in the $T = 100$-mm vessel also show the inclination of the impeller stream and the development of the trailing vortex structure with increasing impeller blade angle noted previously. The highest k level (greater than $0.16V_{tip}^2$) that signifies the presence of the trailing vortex is evident in Figures 16b and 16c. The formation of the trailing vortex associated with the passage of the impeller blades is represented in Figure 16b ($\phi = 15°$) by the highest level of k spreading outward from the impeller tip. This region of high turbulence energy increases in size with increasing impeller blade angle, gradually moving outward both axially and radially, as expected from the rms velocity contours for the 294-mm vessel (Figure 15). The large region of high k shown in Figure 16a for $\phi = 0°$ is associated with the remains of the trailing vortex generated by the previous blade crossing. By comparing the results of Figures 13 and 15, it may be concluded that in general flow features such as the trailing vortex structure and turbulence levels scale well between the two vessels studied.

It should be noted that the angle-resolved (Figure 16) and ensemble-averaged k distributions (Figure 8) are similar at some ϕ angles but not at others. For example, the highest k region (0.08–$0.16V_{tip}^2$) extends radially from 0.19–$0.24T$ at $\phi = 0°$ in Figure 16a, whereas in Figure 8 the highest k region is that where k is greater than $0.16V_{tip}^2$ and it reaches from the blade tip ($0.165T$) to $0.21T$. Conversely, the k contours at $\phi = 15°$ and 30° are more similar to the ensemble-averaged contours. The reason for this is explained below.

Lee et al. (1995) obtained time-resolved LDA measurements in vessels identical to those used in the present study that showed that the velocity realizations were not evenly distributed over the 60° interval between two successive impeller blades. This was due to the existence of a strong correlation between the proportion of data obtained and the impeller blade angle, that is, there was a significant variation of the data rate with ϕ, with over 50% of the velocity realizations recorded occurring within the first 20° of impeller revolution. Hence, it is most likely that 360° ensemble-averaged measurements are most similar to 1° angle-resolved measurements obtained at small blade angles because of the higher concentration of data acquired at these angles. This bias effect results also in profiles of ensemble-averaged mean velocity exhibiting higher values than the equivalent angle-re-

solved mean velocity profiles. Hence, since the impeller pumping capacity (Q) is calculated from the mean velocity profiles, Q and Flow numbers determined from 360° ensemble-averaged mean velocities may be biased toward higher values (Rutherford et al., 1995).

An interesting feature apparent from Figures 15 and 16 is that the respective sets of trailing vortices generated by the upper and lower impellers do not seem to interact with one another. The merging flow pattern is formed by the impeller streams being directed at 45° toward one another due to the proximity of the impellers, but the regions of high k associated with the trailing vortices indicate that the trailing vortex axes do not extend above $z = 0.40T$ (Figure 16a). The influence of the trailing vortex structure has dissipated significantly by $r = 0.30T$ (approximately 1.6 times the impeller blade length) from the center of the vessel, and $z = 0.12T$ above the lower impeller mid-section (approximately 1.7 times the impeller blade height). This is in agreement with the findings of an earlier study by two of the authors (Lee and Yianneskis, 1994) in which a cylindrical region of radius $1.0D$ and height $1.2D$ centered in the middle of the vessel was defined, within which most of the flow periodicity associated with the passage of individual impeller blades would be confined. The vortex axis determined earlier for the merging flow configuration is in agreement with the observation that the trailing vortex structure is contained within a smaller radial distance for a dual-Rushton merging flow configuration than is typical with a single impeller system. This is most likely due to the characteristic inclination of the impeller streams and the strong rotational flow induced by the proximity of the impellers, which lead to a smaller radial spread of the impeller streams than is typical of a single impeller system.

Comparisons of the three turbulent velocity components have shown the turbulence inside this periodic region to be anisotropic ($u' \neq v' \neq w'$). The main consequence of this is that, since many CFD techniques currently use turbulence models based on the assumption of an isotropic flowfield, such models may lead to inaccurate prediction of the levels of k. A number of flow modelers, such as Issa and Gosman (1981), have reported discrepancies between experimental data and predictions obtained from numerical schemes employing the k-ϵ turbulence model. This model is based on an implicit assumption of local isotropy in the turbulence, and is widely used for the prediction of flowfields in stirred vessels. Tatterson (1991) suggested that of the predictions reported that employed the k-ϵ model, those that made use of a three-dimensional nonisotropic version of the model provided the most realistic simulation of the flowfield. Further, Bakker (1992) presented results that showed the k-ϵ model to underpredict turbulence levels in the impeller stream, where the flow has been shown to be anisotropic in the present study, for a vessel agitated by a single Rushton impeller.

The measurements presented in this article suggest that the accuracy of flow predictions in the region near the impellers affected by flow periodicity can be improved by modeling the passage of individual blades in a rotating frame of reference with a nonisotropic turbulence model and assessed against angle-resolved data. Outside the region of flow periodicity, ensemble-averaged values and a stationary frame of reference are more appropriate and the assumption of isotropy may be sufficient. Finally, other flow motions, such as the free surface vortex, that are present in the flows affect the mean velocity and turbulence-level distributions and should be accounted for in the modeling.

Conclusions

Three stable flow patterns generated by two Rushton impellers operating in a stirred vessel have been investigated using a combination of 360° ensemble-averaged and 1° angle-resolved LDA measurements. The 360° ensemble-averaged measurements have been shown to be useful for characterizing the general flow and turbulence characteristics for these stable flow configurations. However, by comparing the two measurement techniques it has also been shown that care must be exercised when interpreting 360° ensemble-averaged data, since in the vicinity of the impellers they may include the periodic fluctuations of the mean velocity introduced by the blade crossings.

Further, the trailing vortex structure produced by the Rushton impellers has been shown to diminish significantly within a region of height $1.0D$ and diameter $1.2D$ around the center of the vessel. Through LDA measurements of all three turbulent velocity components it was established that the turbulence within this region is mostly anisotropic, while outside of this region, in the vessel bulk flow, the turbulence might be considered to be mostly isotropic.

In addition, the effect of vessel scale has been studied and it was found that in general the main flow features such as the impeller stream inclination and turbulence levels scaled well between the two vessels.

Acknowledgments

The authors acknowledge financial support from the Commission of the European Union under the JOULE II Programme Project JOU2-CT92-0127 and the Engineering and Physical Sciences Research Council of the UK under grant GR/H80873.

Notation

U,V,W = axial, radial, and tangential instantaneous velocities, m/s
μ = dynamic viscosity of the fluid, N·s/m^2
ρ = density of the fluid, kg/m^3

Literature Cited

Abbott, M. B., and D. R. Basco, *Computational Fluid Dynamics: An Introduction for Engineers*, Wiley, New York (1989).

Bakker, A., "Hydrodynamics of Stirred Gas-Liquid Dispersions," PhD Thesis, Delft Univ. of Technology, Delft, The Netherlands (1992).

Calabrese, R., and C. M. Stoots, "Flow in the Impeller Region of a Stirred Tank," *Chem. Eng. Prog.*, 43 (May, 1989).

Cooper, R. G., and D. Woolf, "Velocity Profiles and Pumping Capacities for Turbine Type Impellers," *Can. J. Chem. Eng.*, **46**, 94 (1968).

Cutter, L. A., "Flow and Turbulence in a Stirred Tank," *AIChE J.*, **12**(1), 35 (1966).

Issa, R. A., and A. D. Gosman, "The Computation of 3D Turbulent Two-Phase Flows in Mixer Vessels," *Proc. Int. Conf. on Numerical Methods of Lambda Turbulence Flows*, Venice, Italy (1981).

Kuboi, R., and A. W. Nienow, "The Power Drawn by Dual Impeller Systems Under Gassed and Ungassed Conditions," *Proc. Eur. Conf. on Mixing*, Noordwijkerhout, The Netherlands, p. 247 (1982).

Lee, K. C., K. Rutherford, and M. Yianneskis, "A Comparison of Time-Resolved, Angle-Resolved and Ensemble-Averaged LDA Measurements in Stirred Reactors," *Proc. Instn. Chem. Eng. Res. Event*, Edinburgh, Scotland, p. 617 (1995).

Lee, K. C., and M. Yianneskis, "The Extent of Periodicity of the Flow in Vessels Stirred by Rushton Impellers," in *Industrial Mixing Technology: Chemical and Biological Applications*, G. Tatterson, ed., AIChE Symp. Ser., **90**, 5 (1994).

Mahmoudi, S. M. S., *Velocity and Mixing Characteristics of Stirred Vessels with Two Impellers*, PhD Thesis, Univ. of London, London (1994).

Mujumdar, A. S., B. Huang, M. E. Weber, and W. J. M. Douglas, "Turbulence Parameters in a Stirred Tank," *Can. J. Chem. Eng.*, **48**, 475 (1970).

Nouri M., and J. H. Whitelaw, "Effect of Size and Confinement on the Flow Characteristics in Stirred Reactors," *Proc. Int. Symp. on Applied Laser Techniques and Fluid Mechanics*, Lisbon, Portugal, Paper 23.2 (1990).

Revill, B. K., "Pumping Capacity of Disk Turbine Agitators," *Proc. Eur. Conf. on Mixing*, Noordwijkerhout, The Netherlands (April 27–29, 1982).

Rutherford, K., S. M. S. Mahmoudi, K. C. Lee, and M. Yianneskis, "The Influence of Rushton Impeller Blade and Disk Thickness on the Mixing Characteristics of Stirred Vessels," *Trans. Ind. Chem. Eng.*, in press (1996).

Sachs, J. P., and J. H. Rushton, "Discharge Flow from Turbine Type Mixing Impellers," *Chem. Eng. Prog.*, **50**(12), 597 (1954).

Stoots, C. M., and R. V. Calabrese, "The Mean Velocity Field Relative to a Rushton Turbine Blade," *AIChE J.*, **41**(1), 1 (1995).

Tatterson, G. B., *Fluid Mixing and Gas Dispersion in Agitated Tanks*, McGraw-Hill, New York (1991).

van der Molen, K., and H. van Maanen, "Laser Doppler Measurements of the Turbulent Flow in Stirred Vessels to Establish Scaling Rules," *Chem. Eng. Sci.*, **33**, 1161 (1978).

van't Riet, K., and J. M. Smith, "The Behaviour of Gas-Liquid Mixtures Near Rushton Turbine Blades," *Chem. Eng. Sci.*, **28**, 1031 (1973).

van't Riet, K., and J. M. Smith, "The Trailing Vortex System Produced by Rushton Turbine Agitators," *Chem. Eng. Sci.*, **30**, 1093 (1975).

van't Riet, K., W. Bruijn, and J. M. Smith , "Real and Pseudo-Turbulence in the Discharge Stream From a Rushton Turbine," *Chem. Eng. Sci.*, **31**, 407 (1976).

Wu, H., G. K. Patterson, and M. van Doorn, "Distribution of Turbulence Energy Dissipation Rates in a Rushton Turbine Stirred Mixer," *Exp. Fluids*, **8**, 153 (1989).

Yianneskis, M., Z. Popiolek, and J. H. Whitelaw, "An Experimental Study of the Steady and Unsteady Flow Characteristics of Stirred Reactors," *J. Fluid Mech.*, **175**, 537 (1987).

Yianneskis, M., and J. H. Whitelaw, "On the Structure of the Trailing Vortices Around Rushton Turbine Blades," *Trans. Instn. Chem. Eng.*, **71**, Part A, 543 (1993).

Manuscript received Nov. 22, 1994, and revision received Apr. 4, 1995.